AI-Agent-Orchestrated DFT Screening of Conjugated Donor and Electron-Acceptor Building Blocks for Organic Photovoltaics

[1]Igbokwe, Ejikeme Ezo*, [2]Emeka Friday Onu

[1]Department of Physics with Electronics, Ogbonnaya Onu Polytechnic, Aba, Abia State, Nigeria.

[2]Chemistry/Biochemistry department, Ogbonnaya Onu Polytechnic, Aba, Abia State, Nigeria.

Corresponding authors email: ejikeme.igbokwe@ogbonnayaonupolytechnic.edu.ng

Abstract

This study develops and evaluates an AI-agent-orchestrated computational workflow for the preliminary electronic-structure screening of conjugated molecular building blocks relevant to organic photovoltaics (OPVs). A computer-use agent interacts with The structure files and audit spreadsheet are stored in the project archive on the computer. Windows workstation through Remote Desktop Commander (RDC), while RDKit is employed for molecular representation validation, three-dimensional structure generation and molecular mechanics geometry preparation. Quantum-chemical calculations are executed using PySCF within a Linux environment provided by Windows Subsystem for Linux 2 (WSL2). The initial molecular set comprises three oligothiophene-based donor fragments and three electron-deficient heteroaromatic acceptor building blocks, defining nine possible donor–acceptor fragment combinations. Six neutral molecular structures were successfully generated and validated using the ETKDGv3 and MMFF94s procedures. Subsequently, six restricted Kohn–Sham single-point self-consistent-field (SCF) calculations were completed at the B3LYP/6-31G(d) level of theory on the MMFF94s-prepared geometries. All six calculations achieved electronic SCF convergence. The calculated Kohn–Sham HOMO–LUMO gaps ranged from 3.431 to 4.261 eV for the donor fragments and from 3.933 to 4.074 eV for the acceptor fragments. The nine isolated-fragment donor–acceptor comparisons produced acceptor-minus-donor LUMO offsets ranging from −0.702 to −1.736 eV. The six-molecule single-point calculation batch required approximately 388.68 s of wall-clock time. However, no DFT geometry optimization achieved verified convergence, and no validated TD-DFT excited-state results were obtained. Consequently, the reported electronic properties are preliminary single-point descriptors evaluated at molecular mechanics-prepared starting geometries rather than final optimized molecular properties. The study demonstrates the practical integration of AI-assisted computer operation, molecular preparation, quantum-chemical execution, data extraction and preliminary orbital-level analysis. It also establishes the computational foundation for subsequent geometry optimization and excited-state investigations without inferring photovoltaic device performance directly from isolated-molecule calculations.

Keywords: organic photovoltaics; AI agent; computer-use agent; density functional theory; TD-DFT; oligothiophene; benzothiadiazole; molecular screening.

1. Introduction

Organic solar cells (OSCs), also termed organic photovoltaics (OPVs), use conjugated organic semiconductors as photoactive materials. Their performance is influenced by molecular structure,

donor–acceptor pairing, frontier orbital alignment, optical absorption, molecular packing, blend morphology, interfaces and processing conditions [1]. The coupled nature of these factors makes molecular selection a non-trivial task. DFT and TD-DFT provide useful molecular-level tools for examining candidate structures before synthesis, although isolated molecule calculations cannot reproduce the complete solid-state physics of a bulk-heterojunction device [2].

DFT calculations can optimize molecular geometries and estimate ground-state electronic properties. TD-DFT can estimate vertical excitation energies and oscillator strengths [3]. Calculations on neutral and charged states can provide estimates of ionization potentials, electron affinities and internal reorganization energies [4]. These descriptors can support the prioritization of candidate molecules, but they should not be equated with experimental charge mobility, exciton dissociation yield or power-conversion efficiency.

A recent DFT/TD-DFT investigation by Zaier, Martel and Antosiewicz (2023) demonstrated the relevance of oligothiophene donor cores and benzothiadiazole-based π-spacers for OSC molecular design. That work also illustrates why functional selection and comparison with experimental reference data are important when interpreting calculated orbital and optical properties [5]. The present study takes a complementary practical approach: rather than training a machine-learning model, an AI computer-use agent coordinates the actual desktop workflow used to prepare structures, launch quantum-chemistry calculations, monitor execution, extract results and assemble reproducibility records.

The specific objectives of this study are to: Develop and evaluate an AI-agent-assisted computational workflow for coordinating molecular preparation, quantum-chemical calculations, output monitoring and data extraction. Select and validate representative oligothiophene donor fragments and electron-deficient heteroaromatic acceptor building blocks relevant to organic photovoltaic material design. Generate three-dimensional molecular starting geometries using RDKit ETKDGv3 and MMFF94s geometry preparation. Perform B3LYP/6-31G(d) single-point electronic-structure calculations and extract the corresponding frontier molecular orbital energies, Kohn–Sham orbital gaps, total energies and dipole moments. Compare the isolated-fragment frontier orbital energy levels across nine possible donor–acceptor combinations using explicitly defined energy-offset conventions. Evaluate the computational execution performance, calculation completion rate, processing time and reproducibility characteristics of the AI-agent-assisted workflow. Establish the computational requirements for subsequent DFT geometry optimization, TD-DFT excited-state calculations and more comprehensive donor–acceptor investigations.

2. Computational Methodology

2.1 Research design and AI-agent execution architecture

The work is an original computational investigation, not a review paper. Remote Desktop Commander provides the remote computer-operation interface through which the AI agent interacts with the computer. The agent is responsible for application and file operations, launching Python scripts, initiating quantum-chemical jobs, monitoring execution, reading output files and preparing

analysis artefacts. The quantum-mechanical calculations themselves are performed by PySCF. The AI agent does not replace the DFT method and does not train a new machine-learning model.

2.2 Computing environment

The host computer runs Windows 11 Pro (64-bit) and exposes an Ubuntu WSL2 environment. The detected host processor is an Intel Core Ultra 5 125U with 12 cores and 14 logical processors. The workstation reports approximately 7.5 GB of physical memory. The verified WSL2 computational environment uses Python 3.12.16, PySCF 2.14.0 and RDKit 2026.09.1. The host-side structure-preparation environment uses RDKit 2026.09.2. The geomeTRIC 1.1.1 and ASE 3.29.0 packages were installed into the WSL2 environment to support geometry optimization and workflow handling. Software versions will be retained in the final reproducibility record.

2.3 Molecular model selection

A resource-conscious fragment-level screen was defined using three oligothiophene donor models and three electron-deficient heteroaromatic acceptor building blocks. The molecules were selected to represent electron-rich thiophene-based conjugated units and electron-poor heteroaromatic motifs relevant to donor–acceptor organic semiconductor design [5]. The selected structures are molecular building blocks, not complete commercial donor polymers or fullerene/non-fullerene acceptor materials. This limitation is explicitly preserved in the interpretation of the results [6].

The six molecular fragments selected for this investigation comprise three oligothiophene-based donor candidates and three electron-deficient heteroaromatic acceptor candidates. Their molecular identities, PubChem compound identifiers, molecular formulae and respective roles in the screening process are presented in Table 1.

Table 1. Selected donor and acceptor molecular fragments and their molecular characteristics.

Role	Molecule	PubChem CID	Formula	Model description
Donor	2,2'-bithiophene	68120	C8H6S2	Oligothiophene fragment
Donor	2,2':5',2''-terthiophene	65067	C12H8S3	Oligothiophene fragment
Donor	5-ethynyl-terthiophene	13113979	C14H8S3	Substituted oligothiophene fragment
Acceptor	2,1,3-benzothiadiazole	67502	C6H4N2S	Electron-deficient heteroaromatic block
Acceptor	2,1,3-benzoxadiazole	67501	C6H4N2O	Electron-deficient heteroaromatic block
Acceptor	2,1,3-benzothiadiazole-5-carboxylic acid	602011	C7H4N2O2S	Functionalized acceptor block

2.4 Molecular structure preparation and validation

Canonical SMILES records were obtained from PubChem records identified by compound name and CID. RDKit was used to parse each SMILES representation, add explicit hydrogen atoms, generate a three-dimensional conformer with the ETKDGv3 procedure and perform an MMFF geometry preparation. The resulting structures were exported as SDF and XYZ files [7]. A structure audit compared the RDKit-calculated molecular formula with the formula recorded for each PubChem entry [8]. All six candidate SMILES strings parsed successfully, all six three-dimensional structures were generated, all six molecular formulas matched the target formulas, and MMFF optimization returned status 0 for each candidate. The MMFF geometries are starting structures only; they are not treated as DFT-optimized geometries [9].

2.5 DFT electronic-structure calculations

Ground-state electronic-structure calculations were performed using the PySCF quantum-chemistry package. The B3LYP exchange–correlation functional and 6-31G(d) basis set were employed for all six neutral molecular fragments [10]. Restricted Kohn–Sham calculations were conducted using the molecular coordinates obtained from the preceding RDKit ETKDGv3 and MMFF94s structure-preparation procedures.

The numerical integration grid was set to level 1 for the completed single-point calculations [11]. Electronic self-consistent-field convergence was assessed from the native PySCF output. A calculation was classified as electronically converged when the SCF procedure satisfied its convergence criterion and returned a valid final electronic solution [12].

The highest occupied molecular orbital (HOMO) and lowest unoccupied molecular orbital (LUMO) eigenvalues were extracted from the converged Kohn–Sham calculations. The orbital energy difference was calculated as:

$$E_{g,orb} = \varepsilon_{\mathrm{HOMO}} - \varepsilon_{\mathrm{LUMO}} \quad (1)$$

Where:

- $E_{g,orb}$ = HOMO–LUMO orbital energy gap (eV).
- $\varepsilon_{\mathrm{HOMO}}$ = Energy of the highest occupied molecular orbital (eV).
- $\varepsilon_{\mathrm{LUMO}}$ = Energy of the lowest unoccupied molecular orbital (eV).

represent the corresponding Kohn–Sham orbital eigenvalues. Molecular dipole moments and total electronic energies were also extracted [13].

Importantly, the reported calculations were single-point electronic-structure calculations performed on MMFF94s-prepared starting geometries. No molecular fragment achieved verified convergence in a subsequent DFT geometry optimization. Therefore, the reported orbital energies, orbital gaps and dipole moments are preliminary geometry-dependent descriptors and must not be interpreted as final properties of DFT-optimized molecular structures.

A subsequent computational stage will involve DFT geometry optimization, followed by higher-accuracy single-point calculations on the optimized structures. The resulting properties will be compared with the preliminary values reported in this study [14].

.

2.6 Optical excitation properties

Time-dependent density functional theory (TD-DFT) was identified as the intended method for investigating the excited-state electronic properties of the selected molecular fragments. The planned calculations involve obtaining vertical excitation energies and oscillator strengths, which can subsequently be used to estimate molecular absorption wavelengths according to:

$$\lambda = \frac{1239.841984}{E_{\mathrm{exc}}} \qquad (2)$$

However, the exploratory TD-DFT calculations undertaken during the present computational campaign did not produce verified excited-state results [15]. Consequently, no excitation energies, oscillator strengths, absorption wavelengths or simulated optical spectra are reported. The Kohn–Sham HOMO–LUMO orbital gaps obtained from the ground-state calculations are not substituted for optical excitation energies [16].

Validated TD-DFT calculations will form part of the subsequent computational investigation after successful DFT geometry optimization of the molecular structures.

2.7 Donor–acceptor energy-level comparison

The three donor fragments and three acceptor fragments define nine pairwise combinations for comparative energy-level analysis. The comparison uses donor and acceptor HOMO/LUMO energies, orbital gaps, optical transitions and, where completed, ionization potentials, electron affinities and reorganization energies [1]. Energy offsets will be reported with an explicit sign convention [17]. Isolated-fragment alignment is a screening indicator only; it does not establish interfacial charge transfer, blend morphology, charge mobility or device performance [18]. Any donor–acceptor complex calculation will be reported separately with its geometry and interaction-energy definition.

2.8 Agent workflow and reproducibility metrics

The execution record includes the number of structures processed, calculations attempted, SCF convergences, geometry optimizations completed, TD-DFT jobs completed, failures and retries. Quantum-chemical runtime is distinguished from agent/computer-operation time. Every reported numerical value is to be traceable to the corresponding native output file and extraction script.

3. Computational Results and Verification Status

The initial molecular preparation and ground-state electronic-structure calculation stages were completed for six selected molecular fragments. RDKit was used to validate the molecular representations, generate three-dimensional starting structures using ETKDGv3 and perform MMFF94s geometry preparation. All six molecular structures passed the molecular formula validation procedure, and MMFF94s optimization returned status 0 for every candidate [19].

Subsequently, six restricted Kohn–Sham single-point calculations were successfully executed using PySCF at the B3LYP/6-31G(d) level of theory. All six calculations achieved electronic SCF convergence. The calculations were performed on the MMFF94s-prepared starting geometries rather than DFT-optimized structures.

The calculated Kohn–Sham HOMO–LUMO gaps were 4.261 eV for 2,2'-bithiophene, 3.558 eV for 2,2':5',2"-terthiophene and 3.431 eV for 5-ethynyl-2,2':5',2"-terthiophene. For the acceptor fragments, the calculated orbital gaps were 4.037 eV for 2,1,3-benzothiadiazole, 4.074 eV for 2,1,3-benzoxadiazole and 3.933 eV for 2,1,3-benzothiadiazole-5-carboxylic acid.

The resulting frontier orbital energies were used to construct nine isolated-fragment donor–acceptor energy-level comparisons. All nine acceptor-minus-donor LUMO offsets were negative, ranging from −0.702 to −1.736 eV. These results describe the relative Kohn–Sham orbital eigenvalues of the isolated molecular fragments and do not directly establish interfacial charge-transfer energies or photovoltaic performance.

The six-molecule single-point calculation batch required 387.10 s of cumulative per-molecule computational time and 388.68 s of batch wall-clock time. Although all six electronic SCF calculations converged, DFT geometry optimization completion remained 0/6. Similarly, no TD-DFT excited-state calculation produced a verified result.

Accordingly, the completed computational stage establishes a functional workflow for molecular structure preparation, ground-state single-point calculations, frontier orbital extraction and preliminary donor–acceptor orbital-level comparisons. Geometry optimization and excited-state calculations remain outstanding.

4. Results and Discussion

Data-status statement

All six neutral fragments completed converged B3LYP/6-31G(d) single-point SCF calculations. The coordinates were ETKDGv3/MMFF94s-prepared starting geometries. No DFT geometry optimization completed for any of the six molecules. Thus, all orbital energies, gaps and dipoles are preliminary single-point properties at the starting geometries, not final optimized molecular properties [14]. No TD-DFT excited-state calculation completed; no excitation energy, wavelength or oscillator strength is reported.

4.1 Geometry preparation, optimization and convergence

RDKit ETKDGv3 generated three-dimensional structures and MMFF94s geometry preparation returned status 0 for all six candidates; formulas matched the target formulas. These validate structure preparation, not DFT geometry convergence. DFT geometry-optimization attempts did not produce a verified converged optimized structure: 0/6. All six ground-state SCF calculations converged electronically: 6/6. SCF convergence is not evidence that the nuclear geometry is a DFT minimum [12].

All six molecular candidates successfully passed the RDKit structure preparation and MMFF94s geometry preparation procedures, with their calculated molecular formulae matching the corresponding reference structures. However, none achieved verified convergence during DFT geometry optimization, although all six single-point SCF calculations converged electronically. A summary of the molecular preparation and computational convergence status is presented in Table 2.

Table 2. Molecular structure preparation and computational convergence status of the six selected molecular fragments.

Molecule	Formula	MMFF94s prep	DFT geometry	SCF
2,2'-bithiophene	C8H6S2	Status 0	Not optimized	Converged
2,2':5',2''-terthiophene	C12H8S3	Status 0	Not optimized	Converged
5-ethynyl-2,2':5',2''-terthiophene	C14H8S3	Status 0	Not optimized	Converged
2,1,3-benzothiadiazole	C6H4N2S	Status 0	Not optimized	Converged
2,1,3-benzoxadiazole	C6H4N2O	Status 0	Not optimized	Converged
2,1,3-benzothiadiazole-5-carboxylic acid	C7H4N2O2S	Status 0	Not optimized	Converged

Note: MMFF94s status 0 indicates successful molecular mechanics geometry preparation. SCF convergence refers to electronic convergence and does not establish DFT geometry optimization.

4.2 Frontier molecular orbitals and dipole moments

The converged B3LYP/6-31G(d) single-point calculations were used to obtain the total electronic energies, highest occupied molecular orbital (HOMO) energies, lowest unoccupied molecular orbital (LUMO) energies and molecular dipole moments of the six selected fragments. The corresponding Kohn–Sham orbital gaps were calculated as the difference between the LUMO and HOMO eigenvalues. The resulting electronic properties are summarized in Table 3.

Table 3. Calculated single-point electronic properties of the selected donor and acceptor molecular fragments at the B3LYP/6-31G(d) level of theory.

Molecule	Formula	E (Eh)	HOMO (eV)	LUMO (eV)	Gap (eV)	Dipole (D)
2,2'-bithiophene	C8H6S2	-1104.801284	-5.423	-1.162	4.261	1.032
2,2':5',2''-terthiophene	C12H8S3	-1656.610617	-5.125	-1.567	3.558	0.560
5-ethynyl-2,2':5',2''-terthiophene	C14H8S3	-1732.752551	-5.202	-1.770	3.431	1.323

2,1,3-benzothiadiazole	C6H4N2S	-738.702304	-6.509	-2.472	4.037	2.102
2,1,3-benzoxadiazole	C6H4N2O	-415.664057	-6.715	-2.642	4.074	4.254
2,1,3-benzothiadiazole-5-carboxylic acid	C7H4N2O2S	-927.269824	-6.832	-2.899	3.933	0.703

Note: All values were calculated using MMFF94s-prepared starting geometries without subsequent DFT geometry optimization. E is the total electronic energy in Hartree (Eh), and the orbital gap is expressed in electronvolts (eV). Dipole moments are reported in Debye (D).

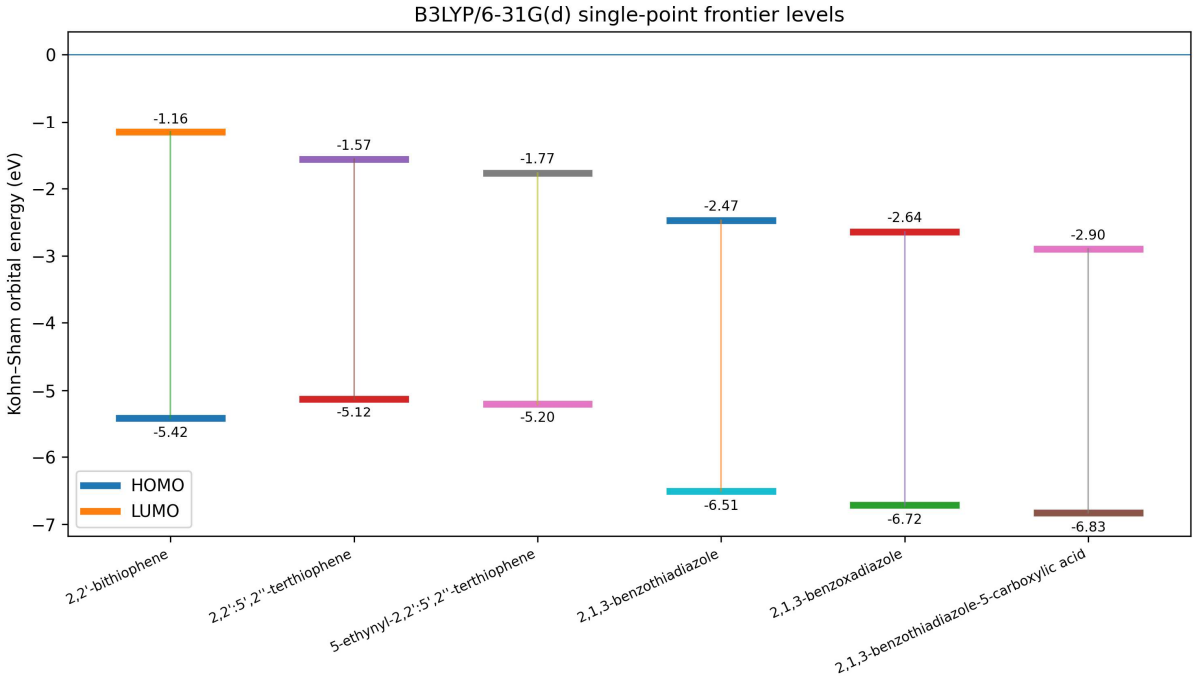


Figure 1. Frontier Kohn–Sham orbital energies from single-point calculations on MMFF94s starting geometries; connectors show orbital eigenvalue differences, not optical transitions.

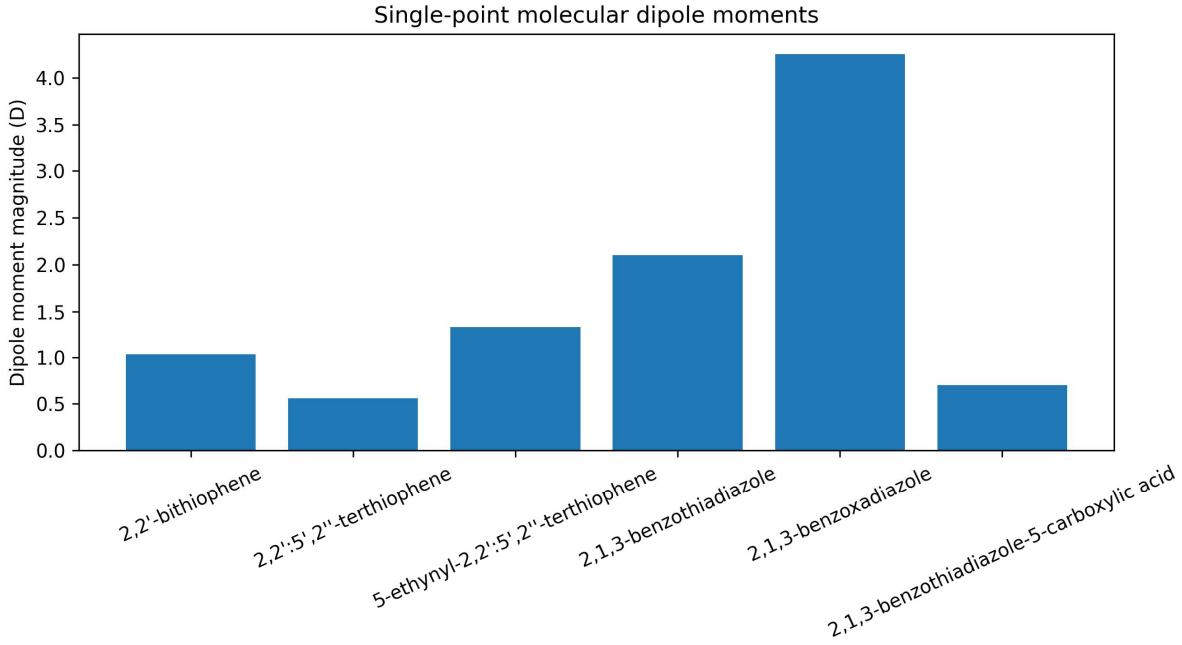


Figure 2. Molecular dipole moment magnitudes from the same single-point calculations.

4.3 Optical excitation properties

No TD-DFT excitation energy, wavelength or oscillator strength passed output verification. Exploratory TD-DFT runs on bithiophene were stopped before an excited-state result was returned. Therefore, no validated optical transition or simulated absorption spectrum is included. The ground-state HOMO–LUMO gaps must not be substituted for TD-DFT excitation energies.

4.4 Nine donor–acceptor fragment alignment comparisons

Three donors were crossed with three acceptors. $\Delta E(LUMO)=\varepsilon_{LUMO}(A)-\varepsilon_{LUMO}(D)$; negative values mean the isolated acceptor LUMO lies below the donor LUMO. $\varepsilon LUMO(A)-\varepsilon HOMO(D)$ is also shown. These are isolated-fragment orbital-level descriptors, not interface charge-transfer energies, binding energies or direct predictions of charge separation.

To examine the relative frontier orbital energy levels of the selected molecular fragments, the three donor candidates were paired computationally with the three acceptor candidates, producing nine donor–acceptor combinations. The acceptor-minus-donor LUMO energy offset, ΔE(LUMO), was calculated for each combination using the isolated-fragment orbital energies. The resulting energy-level comparisons are presented in Table 4.

Table 4. Frontier molecular orbital energy alignment for the nine donor–acceptor fragment combinations.

Donor	Acceptor	D HOMO	D LUMO	A LUMO	ΔLUMO A−D	A LUMO−D HOMO
2,2'-	2,1,3-	-5.423	-1.162	-2.472	-1.309	2.952

bithiophene	benzothiadiazole					
2,2'-bithiophene	2,1,3-benzoxadiazole	-5.423	-1.162	-2.642	-1.479	2.782
2,2'-bithiophene	2,1,3-benzothiadiazole-5-carboxylic acid	-5.423	-1.162	-2.899	-1.736	2.525
2,2':5',2''-terthiophene	2,1,3-benzothiadiazole	-5.125	-1.567	-2.472	-0.905	2.653
2,2':5',2''-terthiophene	2,1,3-benzoxadiazole	-5.125	-1.567	-2.642	-1.075	2.483
2,2':5',2''-terthiophene	2,1,3-benzothiadiazole-5-carboxylic acid	-5.125	-1.567	-2.899	-1.332	2.226
5-ethynyl-2,2':5',2''-terthiophene	2,1,3-benzothiadiazole	-5.202	-1.770	-2.472	-0.702	2.730
5-ethynyl-2,2':5',2''-terthiophene	2,1,3-benzoxadiazole	-5.202	-1.770	-2.642	-0.871	2.560
5-ethynyl-2,2':5',2''-terthiophene	2,1,3-benzothiadiazole-5-carboxylic acid	-5.202	-1.770	-2.899	-1.129	2.303

Note: ΔE(LUMO) = εLUMO(A) − εLUMO(D), where A and D represent the acceptor and donor, respectively. Negative values indicate that the isolated acceptor LUMO eigenvalue is lower than the corresponding donor LUMO eigenvalue. All energies are expressed in eV. These values represent isolated-fragment orbital-level descriptors and are not direct measurements of interfacial charge-transfer energies.

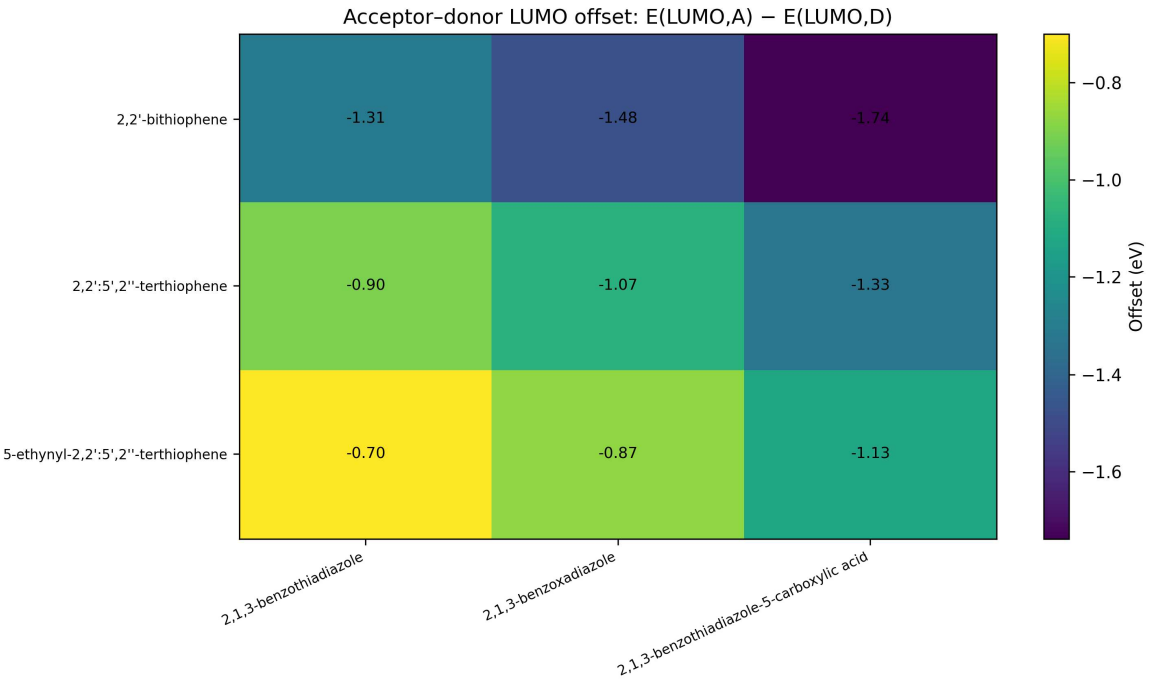


Figure 3. Heatmap of the nine donor–acceptor LUMO offsets, all derived from isolated-fragment single-point calculations.

4.5 AI-agent workflow performance and execution statistics

The six-fragment single-point batch completed 6/6 SCF jobs (100%). The sum of per-molecule elapsed times was 387.10 s (6.45 min); batch wall-clock runtime was 388.68 s. DFT geometry optimization completion was 0/6 and completed TD-DFT jobs were 0. The workflow therefore demonstrates automated molecular preparation, six converged ground-state SCF calculations, data extraction, pairwise analysis and figure generation, but not a complete optimized-geometry/optical campaign.

Remote Desktop Commander cumulative usage snapshot: 773 total tool calls; 765 successful; 8 failed; 99% reported success rate; 17 unique tools; 8 sessions. Most-used actions: read_process_output 427; start_process 191; write_file 43; read_file 39; list_directory 23. These are cumulative tool-usage statistics, not counts of independent scientific calculations.

Per-molecule SCF elapsed times (seconds): 12.04, 151.77, 186.19, 8.83, 7.44 and 20.83 in the order listed in Table 1.

Interpretation and limitations

All nine acceptor-minus-donor LUMO offsets are negative for this fragment set, with magnitudes dependent on the selected donor and acceptor. These gas-phase results omit DFT geometry relaxation, solvent/environment polarization, solid-state packing, intermolecular interface geometry and interface dipoles. They do not establish charge-transfer yield, mobility, morphology or photovoltaic efficiency [19].

5. Limitations of the Study

Several limitations should be considered when interpreting the results of this preliminary computational investigation.

First, the molecular screening was conducted using relatively small conjugated building blocks rather than complete donor polymers and established non-fullerene acceptor materials. Finite oligothiophene fragments cannot fully represent the electronic structure, conformational distribution and extended conjugation of polymeric donor materials. Similarly, the selected heteroaromatic acceptors represent molecular building blocks rather than complete photovoltaic acceptor systems.

Second, although all six molecular structures passed the initial RDKit and MMFF94s geometry-preparation procedures, none achieved verified convergence in DFT geometry optimization. The reported electronic properties were therefore calculated using molecular mechanics-prepared starting geometries. Because molecular conformation and bond geometry can influence frontier orbital energies and dipole moments, the reported values should be regarded as preliminary descriptors. Subsequent DFT optimization may alter the calculated properties and the relative ordering of the molecular candidates.

Third, the calculations employed the B3LYP functional and 6-31G(d) basis set for isolated neutral molecules in the gas phase. The resulting Kohn–Sham orbital energies are method-dependent and do not directly represent experimentally measured ionization potentials, electron affinities or fundamental quasiparticle energy gaps. In addition, the calculated orbital gaps should not be interpreted as optical excitation energies.

Fourth, the isolated-fragment donor–acceptor comparisons do not explicitly account for intermolecular complex formation, molecular packing, dielectric screening, solvent polarization, interfacial electrostatics or charge-transfer-state formation. Consequently, the calculated LUMO offsets cannot independently establish charge-transfer efficiency, exciton dissociation, charge mobility or photovoltaic device performance.

Fifth, no validated TD-DFT calculations were completed. Therefore, the present investigation does not provide verified excited-state energies, oscillator strengths or simulated absorption spectra. Optical properties require additional excited-state calculations and, where possible, comparison with experimental reference data.

Finally, the computational execution was conducted on a resource-constrained desktop workstation. The available memory and processing resources limited the extent of geometry optimization and excited-state calculations that could be completed during the present study. The reported AI-agent execution statistics describe computer-operation activity and should not be interpreted as independent scientific calculation counts.

Future investigations should address these limitations through verified DFT geometry optimization, higher-level electronic-structure calculations where computationally feasible, TD-DFT analysis, charged-state calculations, donor–acceptor complex modelling and comparison with relevant experimental data.

6. Conclusion

This study demonstrated the feasibility of an AI-agent-assisted workflow for the preliminary DFT screening of organic photovoltaic donor and acceptor fragments. Six molecular structures were successfully prepared using RDKit ETKDGv3 and MMFF94s, and all six B3LYP/6-31G(d) single-point SCF calculations converged. The calculated HOMO–LUMO gaps ranged from 3.431 to 4.261 eV for the donor fragments and 3.933 to 4.074 eV for the acceptors. The nine donor–acceptor comparisons produced negative LUMO offsets ranging from −0.702 to −1.736 eV, indicating lower calculated LUMO levels for the acceptor fragments.

The computational workflow achieved 100% SCF convergence, with a batch execution time of approximately 388.68 seconds. However, no DFT geometry optimization or validated TD-DFT calculation was completed. Therefore, the reported electronic properties remain preliminary single-point results based on MMFF94s-prepared geometries and cannot establish optical absorption characteristics or photovoltaic performance. Further work will focus on geometry optimization, recalculation of electronic properties and TD-DFT analysis to provide a more reliable assessment of the selected molecular fragments.

References

1. M. S. Haque and S. Y. Foo, “Donor–Acceptor Interactions in Organic Solar Cells: Linking Molecular Design, Energy-Level Alignment, and Device Performance,” Energies, vol. 19, no. 14, p. 3246, 2026, doi: 10.3390/en19143246.
2. D. Khlaifia, M. Chemek, and K. Alimi, “DFT/TDDFT approach: an incredible success story in prediction of organic materials properties for photovoltaic application,” Moroccan Journal of Chemistry, vol. 8, no. 3, 2020, doi: 10.48317/imist.prsm/morjchem-v8i3.18518.
3. C. Adamo and D. Jacquemin, “The calculations of excited-state properties with Time-Dependent Density Functional Theory,” vol. 42, no. 3, pp. 845–856, 2013, doi: 10.1039/c2cs35394f.
4. T. Ando, N. Shimizu, N. Yamamoto, N. Matsuzawa, H. Maeshima, and H. Kaneko, “Design of Molecules with Low Hole and Electron Reorganization Energy Using DFT Calculations and Bayesian Optimization,” The Journal of Physical Chemistry A, vol. 126, no. 36, pp. 6336–6347, 2022, doi: 10.1021/acs.jpca.2c05229.
5. R. Zaier, A. Martel, and T. J. Antosiewicz, “Effect of Benzothiadiazole-Based π-Spacers on Fine-Tuning of Optoelectronic Properties of Oligothiophene-Core Donor Materials for Efficient Organic Solar Cells: A DFT Study,” The Journal of Physical Chemistry A, vol. 127, no. 50, pp. 10555–10569, 2023, doi: 10.1021/acs.jpca.3c04866.
6. K. H. Lin et al., “Descriptor-Guided Computational Screening of Non-Fullerene Acceptor Cores for Organic Solar Cells,” Advanced Energy Materials, 2026, doi: 10.1002/aenm.71601.
7. S. Wang, G. A. Landrum, J. Witek, and S. Riniker, “Improving Conformer Generation for Small Rings and Macrocycles Based on Distance Geometry and Experimental Torsional-Angle Preferences,” Journal of Chemical Information and Modeling, vol. 60, no. 4, pp. 2044–2058, 2020, doi: 10.1021/acs.jcim.0c00025.
8. D. A. G. Ruiz, B. F. Negrisoli, I. C. C. Periquito, N. M. Nascimento-Júnior, and A. M. Gonçalves, “SMILES2Docking: An Open-Source Desktop Workflow for Ligand Ionization, Stereochemistry-Aware Preparation and Semi-Empirical 3D Refinement,” Molecular Informatics, vol. 45, no. 9, p. e70053, 2026, doi: 10.1002/minf.70053.
9. V. T. Lim, G. Tresadern, C. I. Bayly, D. F. Hahn, and D. L. Mobley, “Benchmark assessment of molecular geometries and energies from small molecule force fields,” F1000Research, vol. 9, p. 1390, 2020, doi: 10.12688/f1000research.27141.1.
10. N. Korol, O. Mulesa, O. Symkanych, and M. V. Slyvka, “Quantum-Chemical Screening of Designed Heterocyclic Polymer Dimers Combined with Small-Data Regression Modeling for Organic Solar Cell Materials,” Solar, vol. 6, no. 4, p. 48, 2026, doi: 10.3390/solar6040048.
11. A. Heßelmann, H. J. Werner, and P. J. Knowles, “Thermochemical evaluation of adaptive and fixed density functional theory quadrature schemes,” The Journal of Chemical Physics, vol. 157, no. 23, 2022, doi: 10.1063/5.0119622.
12. D. Sethio, E. Azzopardi, I. F. Galván, I. F. Galván, and R. Lindh, “A Story of Three Levels of Sophistication in SCF/KS-DFT Orbital Optimization Procedures,” The journal of physical chemistry. A/ The journal of physical chemistry. A., vol. 128, no. 12, pp. 2472–2486, 2024, doi: 10.1021/acs.jpca.3c07647.

13. M. Nakata and T. Maeda, “PubChemQC B3LYP/6-31G*//PM6 dataset: the Electronic Structures of 86 Million Molecules using B3LYP/6-31G* calculations,” 2023, doi: 10.48550/arxiv.2305.18454.
14. M. Bursch, J. M. Mewes, A. Hansen, and S. Grimme, “Best-Practice DFT Protocols for Basic Molecular Computational Chemistry**,” Angewandte Chemie, vol. 134, no. 42, 2022, doi: 10.1002/ange.202205735.
15. S. Ghosh and K. Bhattacharyya, “Origin of the Failure of Density Functional Theories in Predicting Inverted Singlet–Triplet Gaps,” The Journal of Physical Chemistry A, vol. 126, no. 8, pp. 1378–1385, 2022, doi: 10.1021/acs.jpca.1c10492.
16. A. M. Ramadan, M. A. Fouad, and A. A. Hasanein, “Computational study of adsorption and photophysical properties of metallophthalocyanine dyes for DSSCs,” Academia Nano: Science, Materials, Technology, vol. 1, no. 1, 2024, doi: 10.20935/AcadNano7279.
17. K. G. Lim, S. Ahn, and T. W. Lee, “Energy level alignment of dipolar interface layer in organic and hybrid perovskite solar cells,” Journal of Materials Chemistry C, vol. 6, no. 12, pp. 2915–2924, 2018, doi: 10.1039/c8tc00166a.
18. W. Lowrie, J. M. Marín-Beloqui, J. Guo, R. J. E. Westbrook, H. I. Gonev, and T. M. Clarke, “Organic photovoltaics: The current challenges,” The Journal of Chemical Physics, vol. 158, no. 11, 2023, doi: 10.1063/5.0139457.
19. J. S. Müller et al., “Charge-Transfer State Dissociation Efficiency Can Limit Free Charge Generation in Low-Offset Organic Solar Cells,” vol. 8, no. 8, pp. 3387–3397, 2023, doi: 10.1021/acsenergylett.3c00943.